





# SS-IPLE: Semantic Segmentation of Electric Power Corridor Scene and Individual Power Line Extraction From UAV-Based Lidar Point Cloud

Xiuning Liu, Feng Shuang , Yong Li , Liqiang Zhang , Xingwen Huang, and Jianchuang Qin 

**Abstract**—Key objects' semantic segmentation and power line extraction from the electric power corridor point cloud are critical steps in power line inspection. However, the massive amount of point cloud data and missing power line points pose a challenge to the object extraction. To complete the extraction of power lines and other essential objects, a method called SS-IPLE is proposed, which is based on a pointwise multilayer-perceptron semantic segmentation network. The method consists of two main parts: electric power corridor semantic segmentation and individual power line extraction. In the segmentation step, SCF-Net is employed as our primary segmentation network, and the network can process large-scale point clouds. To further improve the segmentation ability of SCF-Net in the corridor, a local coding module is designed to construct the SCFL-Net. In the individual power line extraction step, individual power lines are extracted by flexible grid filtering, effectively overcoming the point-missing problem. The corridor point cloud semantic segmentation and individual power line extraction experiments are conducted in different corridors collected from suburban areas. Promising results are obtained for both semantic segmentation and individual power line extraction, with an mIoU of point cloud semantic segmentation and a mean extraction rate of 96.70% and 96.56%, respectively.

**Index Terms**—Electric power corridor, point cloud semantic segmentation, power line extraction.

## I. INTRODUCTION

A RELIABLE supply of electricity is essential in modern society. As the backbone of the electrical network infrastructure, power lines are continuously exposed to the harsh natural environments, leading to potential failures and damage in electric power corridors. In addition, tree growth close to power lines can also damage electrical networks and lead to bushfires [1]. Therefore, it is necessary to inspect and maintain the power line regularly.

Traditional power line inspection methods are labor-intensive and inefficient. Currently, unmanned aerial vehicle (UAV)-based power line inspection has become a cost-effective and efficient short-distance solution [2]. UAVs provide various data types for power line inspection through remote sensing technologies (such as optical cameras, Lidar, and infrared cameras). The accuracy of power line positioning extracted from the two-dimensional (2-D) observations is limited and requires improvement [3]. Point cloud data obtained from Lidar contains accurate three-dimensional (3-D) coordinate information of objects, which is essential for constructing a 3-D map for UAV power line inspection and accurately measuring the hidden danger area of power targets. Consequently, point cloud data are increasingly used in power line inspection [4].

Power line inspection includes two aspects: assessing the status of power lines and their distance from surrounding potentially threatening objects, such as vegetation and buildings. Therefore, extracting power lines and potential threat objects from point cloud data is the basis of power line inspection. Moreover, semantic segmentation methods can achieve fine classification of the electric power corridor scene. This fine-grained classification enables a more detailed understanding and analysis of the objects within the corridor scene. To achieve comprehensive and refined power line inspection, semantic segmentation of the corridors should be an essential part of the power line extraction process.

In previous studies, the extraction of power lines involves two independent steps: the extraction of candidate power line points and refinement, where individual power lines are extracted from the candidate points [5]. In this study, we adopt a similar approach but replace the candidate power line point extraction

Manuscript received 21 March 2023; revised 31 May 2023 and 19 June 2023; accepted 20 June 2023. Date of publication 26 June 2023; date of current version 14 July 2023. This work was supported in part by the Natural Science Foundation of Guangxi under Grant 2022GXNSFBA035661, in part by the National Natural Science Foundation of China under Grant 42071445, in part by the Guangxi Science and Technology Base and Talent Project under Grant Guike AD22080043, and in part by the Bagui Scholar Program of Guangxi. (Xiuning Liu and Feng Shuang are co-first authors.) (Corresponding author: Yong Li.)

Xiuning Liu, Feng Shuang, Yong Li, Xingwen Huang, and Jianchuang Qin are with the Guangxi Key Laboratory of Intelligent Control and Maintenance of Power Equipment, School of Electrical Engineering, Guangxi University, Nanning 530004, China (e-mail: 2112391036@st.gxu.edu.cn; fshuang@gxu.edu.cn; yongli@gxu.edu.cn; 2112301029@st.gxu.edu.cn; 2112392087@st.gxu.edu.cn).

Liqiang Zhang is with the State Key Laboratory of Remote Sensing Science and the School of Geography, Beijing Normal University, Beijing 100875, China (e-mail: zhanglq@bnu.edu.cn).

Digital Object Identifier 10.1109/JSTARS.2023.3289599

process with semantic segmentation of the corridor. For the extraction of the candidate points, the previous related methods can be broadly classified as supervised and unsupervised according to whether the label is used.

*Unsupervised extraction methods:* In these methods, the point cloud is first divided into grids, and the grid is used as the unit for the candidate power line point extraction. Zhang et al. [6] extracted the candidate points by neighboring grids' height similarity estimation and linear-feature-based clustering. However, a significant number of ground points and vegetation points impact computational efficiency and extraction accuracy. To eliminate this problem, Jung et al. [7] removed the ground surface and adjacent objects before extracting power line points and extracted the candidate points by calculating the similarity of adjacent grids and their internal features. Shi et al. [8] projected the point cloud onto the  $XY$  plane's cell to extract the power line points and pylon points based on the height histogram distribution characteristics of the cell. The above-mentioned grid-based methods are susceptible to the size of the grid and high tree point noise.

*Supervised extraction methods:* Most of the previous methods used traditional classifiers, such as Random Forest, Boost, and support vector machine (SVM) to classify the corridor point cloud and get the candidate power line points. Kim and Sohn [9] constructed 21 features from the sphere domain of points and classified a corridor into power lines, buildings, pylons, ground, and vegetation based on Random Forest. Bo et al. [10] added intensity and echo features based on Kim's method. However, both approaches require constructing too many local features, which results in redundant information. Liu et al. [11] selected the top five 2-D and 3-D features with the best discrimination and combined them into a robust classifier through the AdaBoost algorithm. SVM has also been applied to electric power corridor classification as a classical classifier [12]. These methods have achieved impressive segmentation results in experiments, but building broadly applicable features is still complicated.

Deep learning (DL) has shown good performance in classification [13] and semantic segmentation [14]. DL-based point cloud semantic segmentation methods can be divided into four categories: multiview-based, voxel-based, pointwise-based, and graph-based methods. PointNet [15] aggregates per-point features by max-pooling and causes local information to be missing. Therefore, many methods are proposed to make improvements, such as PointNet++ [16] and PointWeb [17]. These methods cannot directly deal with larger point clouds due to expensive computation and the incapability of capturing structures. To address these problems, RandLA-Net [18] is proposed to solve these two problems by random sampling and expanding the single-point receptive field. However, its ability of local context information extraction is not satisfactory. To address this issue, SCF-Net [19] enhances the ability of RandLA-Net to capture local context information without losing too much computational efficiency. Meanwhile, MSIDA-Net [20] encodes local information in multiple coordinate systems to enhance the local feature expression ability. Although many DL-based semantic segmentation methods have been developed, few are applied in the corridor point cloud. Li et al. [5] proposed a segmentation method based on a graph convolution network, whereas Guan

et al. [21] converted the raw point cloud to cuboids before being fed into the PointNet, achieving high classification accuracy.

For the refinement stage, we review some related works as follows. Some extraction methods are based on the traditional plane line detection algorithm, such as the Hough transform algorithm [22]. On the basis of this algorithm, Guan et al. [23] separated power lines into linear clusters in the  $XY$  plane and then applied a Euclidean distance clustering method to cluster the individual power lines in 3-D space. Lehtomaki et al. [24] used the RANSAC method to detect linear clusters and cluster the individual power lines according to the angle and distance threshold in 3-D space. These methods have an excellent extraction effect but still need to be adapted to address missing power line points and overlapping on the  $XY$  plane.

Other methods mainly extract the individual power lines by clustering and regional growth in 3-D space. In terms of clustering, Peng et al. [25] proposed an individual power line extraction method based on DBSCAN clustering. Similarly, Mao et al. [26] used the distance between power line points and the overall fitting equation of all points as features and applied the DBSCAN clustering algorithm in the feature space to extract individual power lines. Other clustering methods are also applied in the extraction process, Chen et al. [27] constructed a spherical neighborhood for each point, and the individual power lines are separated by conditional Euclidean clustering with constraints of linear features in the spherical neighborhood. In terms of regional growth, Shi et al. [28] selected the lowest elevation point of the power line points as the seed point and extracted individual power lines by a regional growth algorithm with spatial feature constraints. The above-mentioned methods work well to solve overlapping problems, but the missing power line point problem is still a challenge for individual power line extraction.

To sum up, this study aims to propose an automatic power line extraction method based on semantic segmentation of electric power corridors. Our main contributions are as follows.

- 1) A power line extraction algorithm based on pointwise multilayer-perceptron is proposed. Different from the previous extraction algorithms that only extract power lines, the proposed method can precisely implement semantic segmentation of multiple objects in the electric power corridor scene.
- 2) In the corridor semantic segmentation stage, according to the characteristics of the local structure of the corridor point cloud, we propose a local coding module (LCM) that can effectively and fully aggregate a single point's local information to enhance the network's segmentation ability.
- 3) To address the issue of missing power line points, an individual power line extraction method based on a flexible grid is designed. This method is robust against missing power line points and can be applied to various types of power lines.

## II. PROPOSED METHODOLOGY

In this section, we present the power line extraction method named SS-IPLE. The extraction process comprises two steps: electric power corridor semantic segmentation and individual

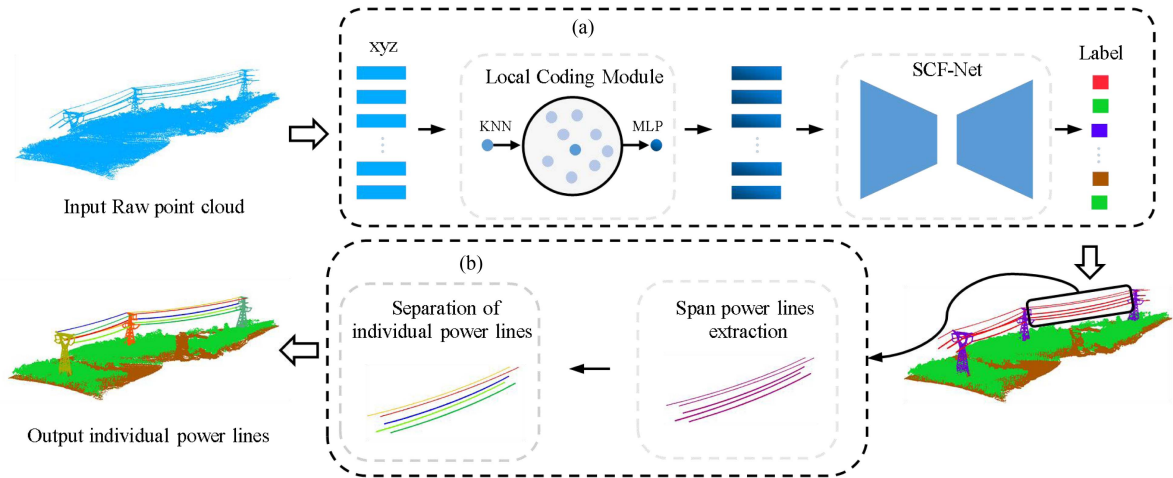


Fig. 1. Flowchart of the proposed method. (a) Electric power corridor semantic segmentation. (b) Individual power line extraction.

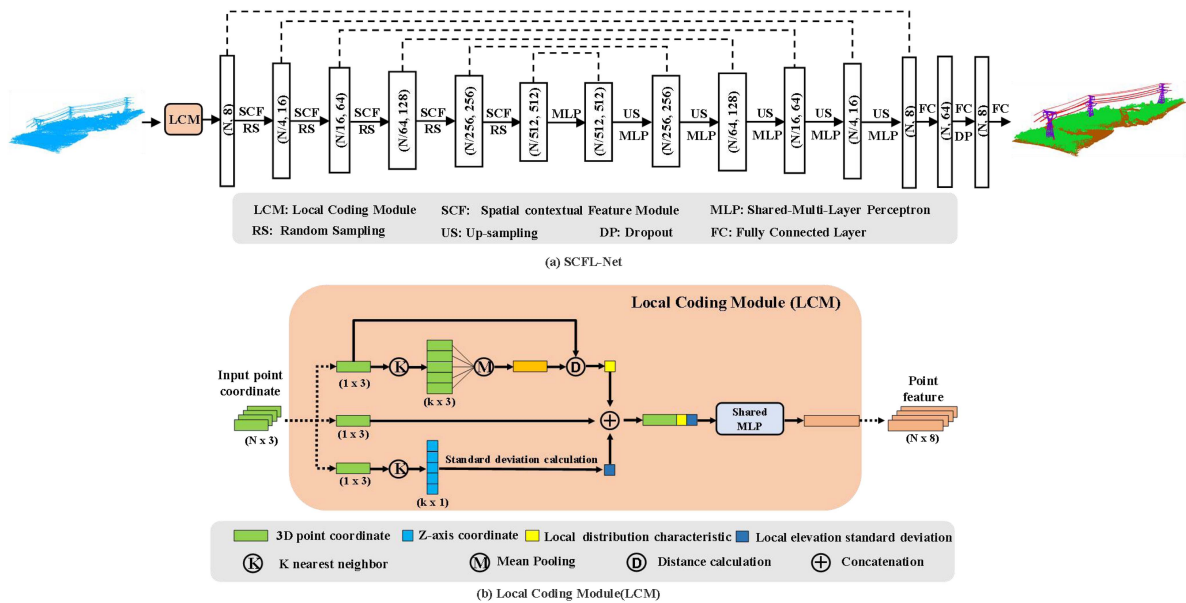


Fig. 2. Architecture of the electric power corridor semantic segmentation network. (a) SCFL-Net. (b) LCM.

power line extraction. In the first step, the corridor point cloud with only  $XYZ$  coordinate information is input and processed by the local coding module (LCM). Subsequently, it is fed into SCF-Net to classify into four categories: ground, vegetation, pylons, and power lines, as shown in Fig. 1(a). In the second step, to accurately extract the individual power lines between two pylons, a two-stage individual power line extraction method is proposed, including span power line extraction and separation of individual power lines, as shown in Fig. 1(b). The details of these two steps are presented below.

#### A. Electric Power Corridor Semantic Segmentation

SCF-Net can effectively learn context features for large-scale point clouds. Here, SCF-Net is used as the basic semantic

segmentation network. To better capture the local structural information of corridors, the LCM is integrated into the SCF-Net to enhance its ability to capture local structural information. This combined segmentation network is named SCFL-Net, as shown in Fig. 2(a). The LCM uses the local interior point distribution and point elevation statistical characteristics to construct local features. A shared MLP is used to map the features to the same dimensional space. In this section, we will introduce the LCM in detail.

1) *Local Distribution Characteristic*: The neighboring point distribution characteristics mainly represent the spatial relationship between a single point and its neighboring points. We express it as the distance between a point and the center of the mass point of the local neighborhood. Generally, if the neighboring points are evenly distributed, the center of mass will be close to

the point. Define a point  $p_i = (x_i, y_i, z_i) \in P$ , where  $P$  is the set of all points, the number of points in the local neighborhood is  $k$ , and a set of neighborhood points  $Q_i = \{p_j\}$ ,  $j = 01, 2 \dots k$  can be obtained by KNN search. The distribution characteristics can be defined as  $Ld_i$ , which is given as follows:

$$Ld_i = \left\| p_i - \frac{\sum_{j=0}^k p_j}{k} \right\| \quad (1)$$

where “ $\|\cdot\|$ ” is the L2 norm.

2) *Local Elevation Standard Deviation*: The local elevation standard deviation is an index that describes the degree of elevation fluctuation in a point cloud. It can effectively quantify the difference in elevation variation between points. A large elevation fluctuation means the local region has a high standard deviation, such as vegetation and pylons. Conversely, slight elevation fluctuation means a lower standard deviation, such as ground and power lines. The expression for elevation standard deviation is given as follows:

$$Lesd_i = \frac{1}{k-1} \sum_{j=0}^k \left( z_j - \frac{\sum_{j=0}^k z_j}{k} \right)^2 \quad (2)$$

where  $z_j$  is the elevation value of  $p_j$ .

Finally, the above-mentioned two features are concatenated with the single-point coordinates, and the local feature information can be mapped to the same feature vector space by using a shared MLP

$$f_i = \text{MLP}((x_i, y_i, z_i) \oplus Ld_i \oplus Lesd_i) \quad (3)$$

where “ $\oplus$ ” is the concatenation operator.  $(x_i, y_i, z_i)$  are the coordinates of  $p_i$ .

In summary, the structure of LCM is shown in Fig. 2(b). It takes all the 3-D point coordinates in the corridor as input and generates an eight-dimensional feature vector that contains local information for each point as output.

### B. Individual Power Line Extraction

Extracting individual power lines from the semantic segmentation results can be divided into two steps: separation of power lines between adjacent pylons and separation of individual power lines. The separation of power lines between adjacent pylons can also be called span power line extraction.

1) *Span Power Line Extraction*: Based on the semantic segmentation results, all the points belonging to pylons and power lines can be extracted. The points corresponding to a pylon can be obtained by using a clustering method. To extract the span power lines accurately and completely, we first project the power lines and the corresponding pylon points onto the  $X$ - $Y$  plane, as depicted in Fig. 3(b). The green line in the enlarged region represents the ideal axis of symmetry of the pylon, which effectively distinguishes the power line points in the span from those belonging to others. Here, we calculate the axis of symmetry of the pylons as follows.

First, a segment of the pylon body is taken vertically from top to bottom to represent the pylon. Assuming that the axis

of symmetry passes through the center point of the pylon, we calculate the average of the pylon’s points to obtain the center point  $(x_0, y_0)$  as shown in Fig. 3(c). The axis of symmetry equation of the pylon can then be expressed as follows:

$$y = \text{line}_{\alpha^*}(x) = x \tan(\alpha^*) + y_0 - x_0 \tan(\alpha^*) \quad (4)$$

where  $\alpha^*$  is the angle between the axis of symmetry and the  $X$ -axis.

On the other hand, the equation of all lines passing through the center point can be expressed as follows:

$$y = \text{line}_{\alpha}(x) = x \tan(\alpha) + y_0 - x_0 \tan(\alpha) \quad (5)$$

where  $\alpha$  is a variable that denotes the angle between a line and the  $X$ -axis.

Second, to determine the equation, we need to find  $\alpha^*$  in  $\alpha$ . This can be achieved by minimizing the variance of distances between all pylon’s points and the line denoted by  $\text{line}_{\alpha}(x)$ . The distance between the  $i$ th point of the pylon and  $\text{line}_{\alpha}(x)$  is represented as  $\text{dis}_i^{\alpha}$ . The variance of distances corresponding to  $\text{line}_{\alpha}(x)$  can be expressed as follows:

$$\text{Var}_{\alpha} = \frac{\sum_{i=1}^N (\text{dis}_i^{\alpha} - \overline{\text{dis}^{\alpha}})^2}{N} \quad (6)$$

where  $\overline{\text{dis}^{\alpha}}$  is the average distance of all pylon’s points from  $\text{line}_{\alpha}(x)$ , and  $N$  is the total number of points in the pylon.

Fig. 3(d) shows the functional relationship between  $\alpha$  and  $\text{Var}_{\alpha}$ . The minimum of  $\text{Var}_{\alpha}$  corresponds to the angle  $\alpha^*$ . To search for  $\alpha^*$ , the golden section search way [29] is utilized within the range of  $\alpha \in [-90^{\circ}, 90^{\circ}]$ .

2) *Separation of Individual Power Lines*: In span power lines, each power line does not overlap and is stratified in the elevation direction. Based on this, an individual power line separation algorithm that utilizes flexible grid filtering is proposed. First, the span power lines are rotated parallel to the  $X$ -axis to reduce computation, and the discrete points are filtered by radius filtering. The algorithm flowchart is illustrated in Fig. 4. The separation module takes the span power lines’ points as input and cyclically separates a single power line until all points are separated. The separation is composed of five steps:

*Step 1*: Plane grid points are generated uniformly according to the defined grid resolution  $res$  (m). The  $Z$ -axis value of each grid point is initialized below the lowest elevation value of the span power line points. Next, the power line points are projected onto the grid surface. Within the adjacent rectangular region of a grid point, the power line points that are projected within this region are designated as the search points set for the grid point. As shown in Fig. 5.

*Step 2*: The upward motion of grid points at a constant speed is simulated by iteratively increasing the  $Z$ -axis value for each grid point. In each iteration, the  $Z$ -axis value of the point is increased by  $(res * rate)$  (m), where the rate is a ratio.

*Step 3*: Motion cessation is determined for each grid point based on the following conditions: the  $Z$ -axis distance between a grid point and the nearest power line point in the corresponding search points set is less than  $(res * rate)$  (m), or the adjacent grid



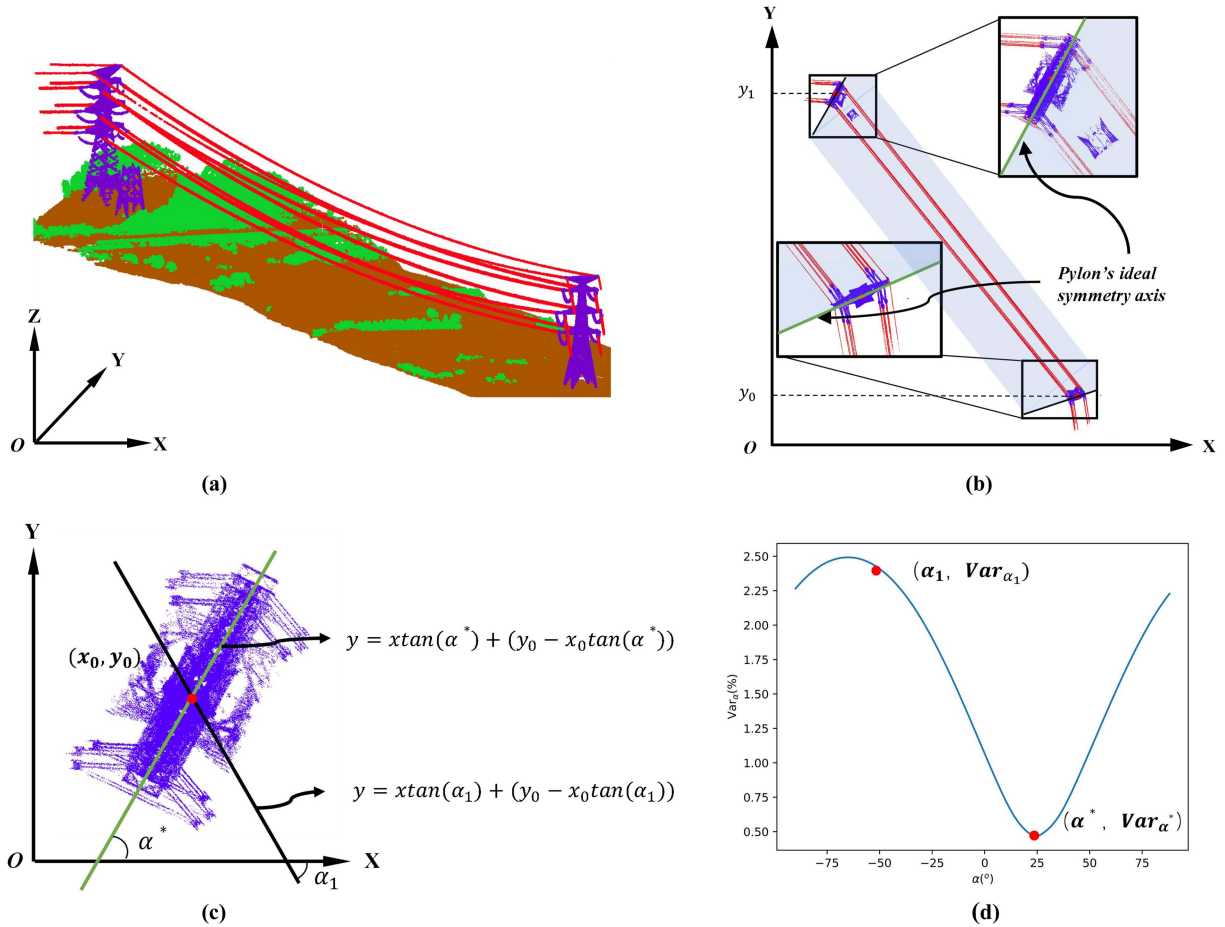


Fig. 3. Span power line extraction. (a) Electric power corridor. (b) Corridor projection onto the X-Y plane. (c) Equation of a line with different angles  $\alpha$  passing through the center of a pylon. (d) Curve between  $\text{Var}_{\alpha}$  and  $\alpha$ .

points have already stopped. Grid points that stop moving due to the former condition are considered elevation reference grid points. The iteration is terminated when all grid points cease motion.

*Step 4:* The Z-axis distance between the power line point and the nearest elevation reference grid point is calculated. The power line points with a Z-axis distance less than the threshold  $h$ (m) are selected as the separated single-layer power line points.

*Step 5:* The extracted single-layer power line is rotated  $90^{\circ}$  along its length. Repeat steps 1–4 to separate a single power line.

To account for the varying section sizes of different layers of power lines, an automatic adjustment of the threshold  $h$  (m) is necessary during the cyclic separation of individual power lines. As shown in Fig. 6, the power line points are projected onto the X-Z plane, and the power line segments are vertically cut around the lowest height point. Subsequently, the threshold  $h$  (m) is adaptively calculated based on the centralized distribution characteristics of the Z-axis values of different layers within the segment.

To further illustrate the implementation process of the algorithm in the separation module, we provide a detailed description of the primary process, as listed in Algorithm 1.

### III. EXPERIMENTS AND ANALYSIS

#### A. Dataset

The power corridor dataset was collected by DJI RTK300 UAV Lidar in Nanning, China. The raw point cloud contains the 3-D coordinate (XYZ) information of points, with a density of about 580 points per square meter. The raw point cloud contains three independent electric power corridors:  $S_0$ ,  $S_1$ , and  $S_2$ . The total length of all corridors is about 3500 m, with a total of 27.4 million points. These corridors include different voltage classes of pylons and various types of power lines. The raw point cloud is divided into a training set and a test set using Cloud Compare software (<https://www.cloudcompare.org/>). The point clouds are categorized into ground, vegetation, pylons, and power lines. The number of points for each category label is shown in Fig. 7. Fig. 8 provides more details about the training and test set division for each corridor. The lengths of the test regions in  $S_0$ ,  $S_1$ , and  $S_2$  are 527, 350, and 404 m, respectively, and include different span areas  $T$ .

Table I presents the detailed parameters of the power lines in each testing span area. The power line lengths and densities varied significantly across different span areas, which can better test the individual power line separation algorithm's robustness.

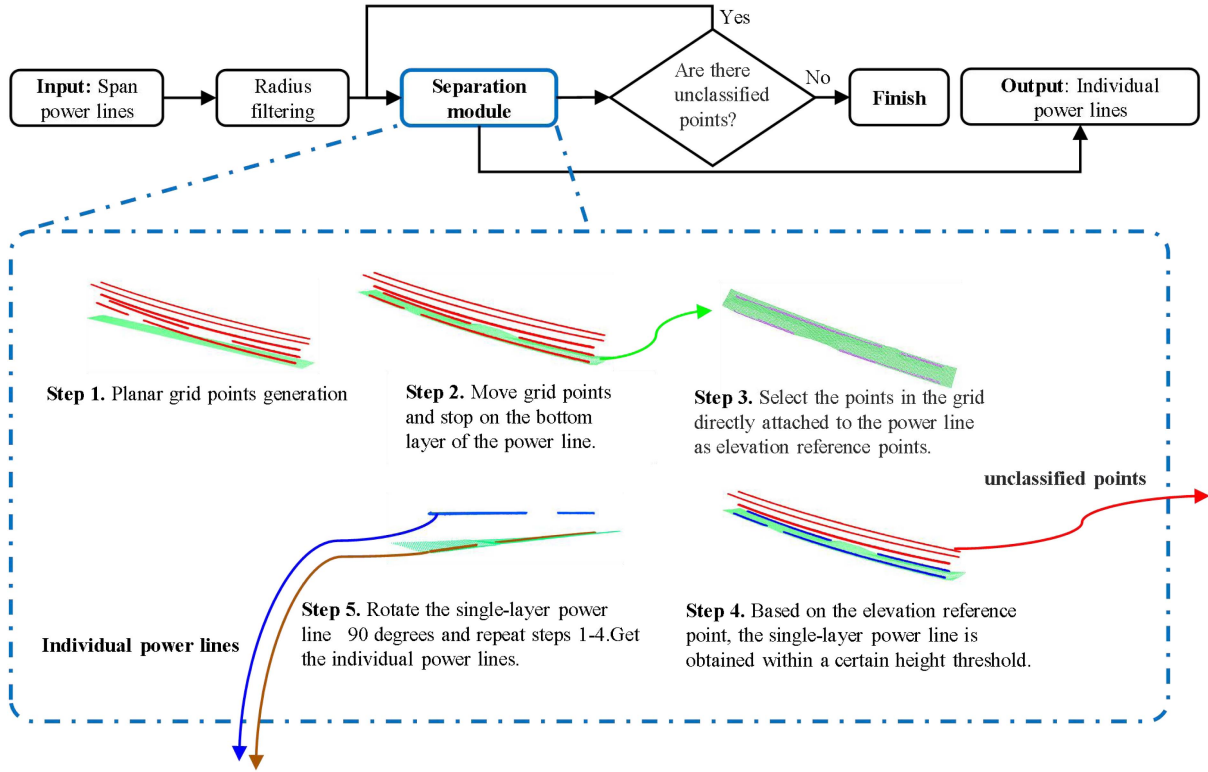


Fig. 4. Overall flowchart of separating individual power lines from a span.

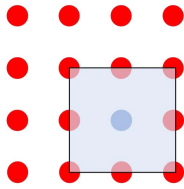


Fig. 5. Adjacent rectangular region. The square area is the blue grid point's adjacent rectangular region.

In this study, the disconnection rate index from [5] is employed to quantify the extent of missing power line points. The disconnection rate is defined as follows:

$$\text{Disconnection rate} = \frac{\text{Disconnection length}}{\text{Total length}} \quad (7)$$

Notably, in  $S_2/T_0$ , the individual power line disconnection rate reaches nearly 36% due to obstructing vegetation, posing a challenge to individual power line extraction, as shown in Fig. 8(c).

### B. Semantic Segmentation on Electric Power Corridor

To evaluate the performance of SCFL-Net in the corridor semantic segmentation, we compare our method with several existing DL-based semantic segmentation algorithms, i.e., PointNet++, RandLA-Net, SCF-Net, BAAF [30], and MSIDA-Net. We apply the same training strategy to all networks to

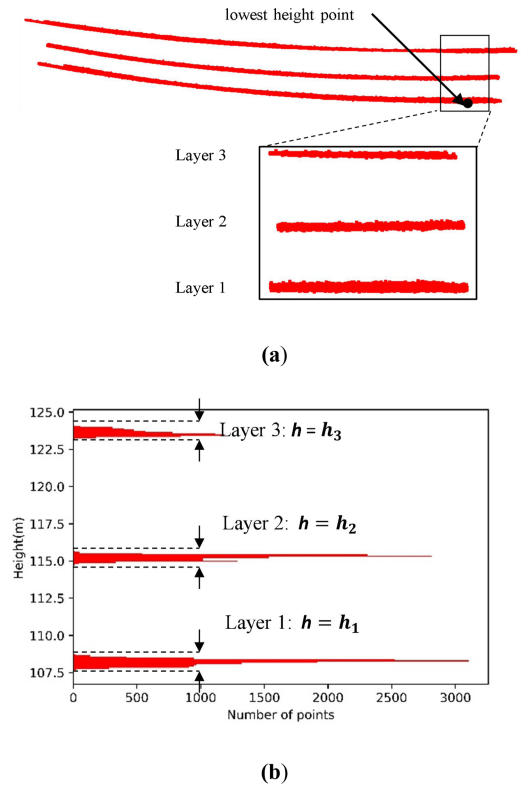


Fig. 6. Adaptive threshold  $h$  calculation. (a) Slices are selected according to the lowest point. (b)  $h$  is calculated based on the elevation distribution of the points.

---

**Algorithm 1:** Individual Power Line Extraction Process Based on Flexible Grid Filter.

---

**Input:** Span power lines points set  
 $\mathbf{Q} = \{(x_i, y_i, z_i) | i = 01, \dots, n\}$

**Output:** Points set  $\mathbf{R}$  selected by the grid filter.

**Parameters:** Grid cell size:  $res$ ; Grid forward rate:  $rate$ ;

```

1   $\mathbf{G} = g(\mathbf{Q}, res) = \{(x_j, y_j, z_j) | j = 01, \dots, m\}$ ;
2  //  $\mathbf{G}$  is a set of grid points,  $g$  is the grid points
   generation function.
3   $\mathbf{H} = h(\mathbf{Q}, \mathbf{G}) = \{max\_z_j | j = 01, \dots, n\}$ ;
4  //  $\mathbf{H}$  is a set of max z-value for each grid point,
    $h$  is the max z-value
5  generating function.
6   $\delta_j = 0 \rightarrow \mathbf{G}$ ;
   //  $\mathbf{G} = \{(x_j, y_j, z_j, \delta_j) | j = 01, \dots, m\}$ 
7  while exist  $\delta_j = 0$  in  $\mathbf{G}$  do :
8     $z_j = z_j + rate * res$ ;
9    for  $j \leftarrow 0; j \leq m$  do :
10   if  $|z_j - max\_z_j| < (rate * res + 0.1)$  then
11      $\delta_j = 1$ ;
12   if exist  $\delta = 1$  in Neighbor grid points then
13      $\delta_j = 2; (x_j, y_j, z_j) \rightarrow \mathbf{G}_{select}$ ;
     //  $\mathbf{G}_{select}$  is a set of grid points
     selected from  $\mathbf{G}$ .
14   end if
15   end for
16   end while
17    $\mathbf{Q}_{Base} = Neighbor\_search(\mathbf{Q}, \mathbf{G}_{select})$ ;
   // Neighbor_search is a function that find the
   nearest distance
18   grid point in set  $\mathbf{G}_{select}$  and make the
   corresponding  $z_j$  as the
19    $h\_base_i$ .  $\mathbf{Q}_{Base} = \{h\_base_i | i = 01, \dots, n\}$ 
20    $h = Adaptive\_gen(\mathbf{Q})$ ;
   // Adaptive_gen is an adaptive generation
   function
21   of threshold  $h$ .
22   for  $i \leftarrow 0; i \leq n$  do :
23     if  $z_i - h\_base_i < h$  then
24        $(x_i, y_i, z_i) \rightarrow \mathbf{R}$ ;
25     end if
26   end for
27   Return  $\mathbf{R}$ ;
```

---

TABLE I  
DETAILS OF THE POWER LINES IN TEST AREA

Test area	Number of lines	Density (point/m)	Average length (m)	Disconnect length (m)	Disconnect rate (%)
$S_0/T_0$	5	134.6	150.41	0.00	0.00
$S_0/T_1$	5	208.1	192.76	0.00	0.00
$S_1/T_0$	8	89.06	516.90	4.90	5.10
$S_2/T_0$	9	238.3	394.59	75.72	35.82

achieve a fair comparison. The initial learning rate is set as 0.02. Within each epoch, the learning rate decays to the original 0.95, the Batch size is 4, and the number of points is 40 960. The training process is deployed on the Quadro RTX 6000 platform with an Intel(R) Core (TM) i9-10900K CPU at 3.70 GHz and 64-GB memory.

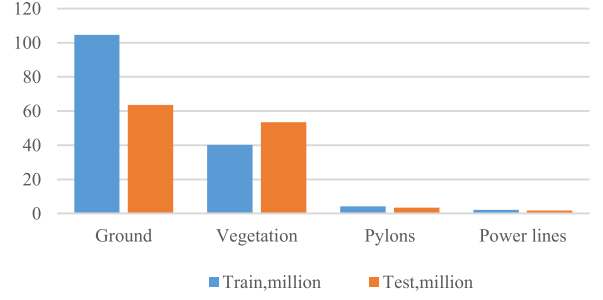


Fig. 7. Statistical diagram of the number of points of each label.

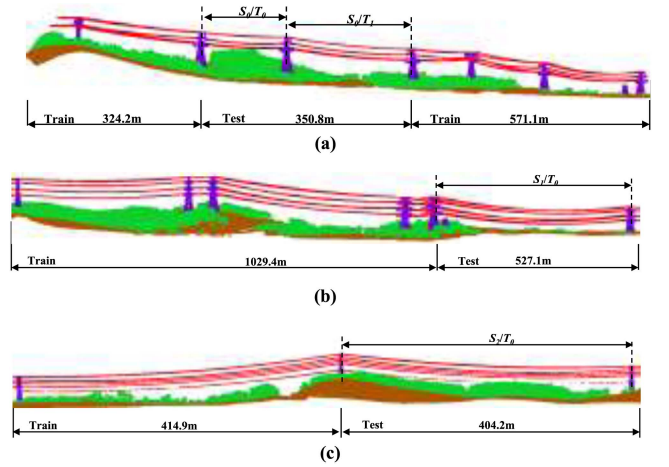


Fig. 8. Each electric power corridor training and test set division. The power lines, pylons, vegetation, and ground are colored in red, purple, green, and brown, respectively. (a) Corridor  $S_0$ . (b) Corridor  $S_1$ . (c) Corridor  $S_2$ .

We use mIoU, OA, and mRec to quantify and evaluate the segmentation effect of our model. OA evaluates the accuracy of point classification. mRec evaluates the recall rate of truth value, and mIoU evaluates the semantic segmentation accuracy of each category

$$OA = \frac{\sum_{i=1}^{n_{class}} TP_i}{N} \quad (8)$$

$$mRec = \sum_{i=1}^{n_{class}} \left( \frac{TP_i}{TP_i + FN_i} \right) / n_{class} \quad (9)$$

$$mIoU = \sum_{i=1}^{n_{class}} \left( \frac{TP_i}{FP_i + FN_i + TP_i} \right) / n_{class} \quad (10)$$

where  $N$  is the total sample,  $TP_i$  is the true-positive sample of class  $i$ ,  $FP_i$  is the false-positive sample of class  $i$ ,  $FN_i$  is the false-negative sample of class  $i$ .  $n_{class}$  is the number of classes.

As listed in Table II, our approach shows a significant advantage over PointNet++. Although the OA of our method only improves by 1.64%, mIoU and mRec increase by 24.42% and 11.25%, respectively. Compared with the recent advanced segmentation methods, our approach achieves the highest segmentation performance with an mIoU of 96.04%. In particular, our approach outperforms SCF-Net with an improvement of

TABLE II  
PERFORMANCE COMPARISONS AMONG DIFFERENT SEGMENTATION METHODS ON POWER LINE DATASET

	OA	mRec	mIoU	Ground	Vegetation	Pylons	Power lines
PointNet++	96.52	86.49	71.62	96.73	94.88	40.81	54.09
RandLA-Net	97.96	96.50	94.77	96.49	95.69	93.65	93.26
BAAF-Net	97.95	96.50	94.85	96.54	95.6	92.39	94.88
MSIDA-Net	97.82	96.46	95.04	96.37	95.22	91.55	<b>97.02</b>
SCF-Net	98.02	96.47	94.74	96.63	95.81	92.87	93.64
SCFL-Net (Ours)	<b>98.16(0.14↑)</b>	<b>97.64(1.17↑)</b>	<b>96.04(1.30↑)</b>	<b>96.76</b>	<b>96.05</b>	<b>95.57</b>	95.78

The best result are highlighted in bold.

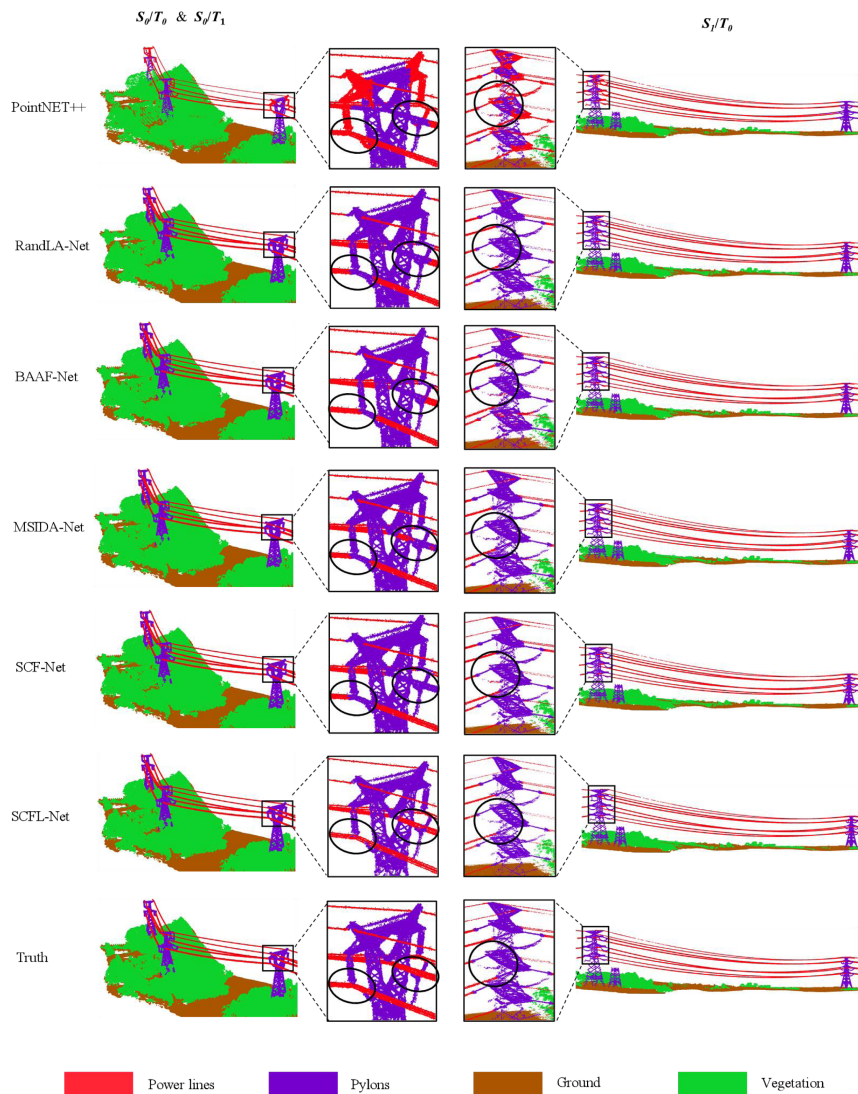


Fig. 9. Segmentation results of  $S_0/T_0$ ,  $S_0/T_1$ , and  $S_1/T_0$ .

1.3% in mIoU, 0.14% in OA, and 1.23% in mRec, indicating that our LCM significantly enhances the segmentation capability of the SCF network. Furthermore, our method achieves the best segmentation of ground, vegetation, and pylon, with IoU reaching 96.76%, 96.05%, and 95.57%, respectively. The critical power line IoU is also above 95%. From the segmentation effect image analysis in Fig. 9, the majority of the misclassified points are located at the junction of the pylon and power lines. This

can be attributed to the presence of structural components, such as insulators in the pylon at the connection point, which are similar to the power lines. The segmentation performance of most comparison methods is not ideal, but SCFL-Net has a good segmentation effect here. This further validates the effectiveness of our LCM in aggregating local distribution features.

The LCM employs a local neighborhood of  $k$  points to capture local distribution features. To determine the optimal value of  $k$ ,



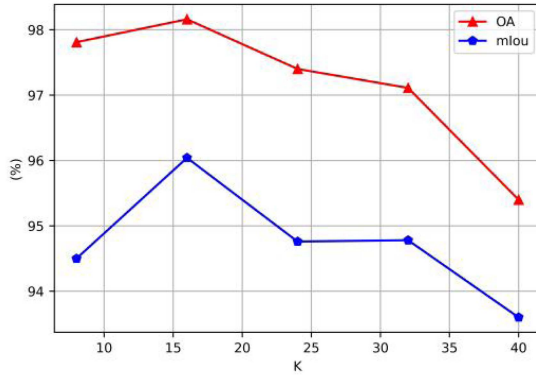


Fig. 10. Segmentation performance under different  $k$  values.

TABLE III  
NUMBER OF PARAMETERS AND TIME CONSUMPTION OF SCFL-NET

	Parameters (millions)	Total time (seconds)	mIoU (%)
RandLA-Net	<b>4.993</b>	<b>114.89</b>	94.77
MIDIS-Net	15.980	161.47	95.04
SCF-Net	12.146	119.39	94.74
SCFL-Net	12.147	119.90	<b>96.04</b>

The best result are highlighted in bold.

we conducted a comparative experiment by selecting different values from the set  $\{8, 16, 24, 32, 40\}$ . The experimental results are shown in Fig. 10. With the increase in neighborhood points, local information is gradually enriched. Both OA and mIoU have been significantly improved. However, beyond a certain point, increasing the number of local points did not yield any further improvement in segmentation performance. The increase in local points cannot provide more local information, and redundant information interference appears, reducing the segmentation performance. Therefore, we choose  $k = 16$  to provide the best semantic segmentation performance.

### C. Efficiency of SCFL-Net

In this section, we systematically evaluate the overall efficiency of our SCFL-Net using the corridor data. To ensure a fair comparison, we conduct experiments on several networks [18], [19], [20] under identical conditions. The number of points put into each network is 40 960 points for one inference. The total time required to complete the inference for all corridors is compared. Table III quantitatively shows the total time of different networks. In addition, the number of parameters for each network is reported to reflect their memory consumption. SCFL-Net exhibits similar efficiency and memory consumption as SCF-Net. However, SCFL-Net is a combination of SCF-Net and LCM, and the proposed LCM only introduces less than 1k parameters compared to SCF-Net, resulting in an improvement in the performance of approximately 1.3%.

### D. Ablation Study on LCM

In order to further demonstrate the contribution of *Local distribution characteristic* (Ld) and *Local elevation standard*

TABLE IV  
RESULTS OF ABLATED NETWORKS

	mIoU (%)
SCF-Net & Ld & Lesd (SCFL-Net)	96.04
SCF-Net & Ld	95.54
SCF-Net	94.74

TABLE V  
RESULTS OF SPAN POWER LINE EXTRACTION

Test Area	Number of power lines points (mill.)	Base on axis of symmetry	
		Precision (%)	Recall (%)
$S_0/T_0$	0.20	100.00	100.00
$S_0/T_i$	0.10	100.00	100.00
$S_1/T_0$	0.37	99.80	100.00
$S_2/T_0$	0.85	100.00	100.00
Average		99.95	100.00

*deviation* (Lesd) in the LCM. Ablation experiments are conducted on the corridor dataset. As shown in Table IV, we first remove the Lesd. The performance reduction from the first row to the second row demonstrates that the Lesd can effectively improve the segmentation performance of the scene. Then, the Ld continues to be removed, and the mIoU is decreased by 0.8%, which demonstrates the effectiveness of Ld.

### E. Span Power Line Extraction and the Axis of Symmetry Equation Search Results

To test the accuracy of the span power line extraction method. The span power line points are manually extracted from the power corridor segmentation results as the correct labels. Note that in the individual power line extraction stage, experiments are conducted on an Intel(R) Core (TM) I9-9900K CPU at a 3.60-GH processor. The algorithms are implemented in Python. Here, precision and recall are used as the evaluation metrics. Table V shows the experimental results for different power line regions. Our method's average precision and average recall are 99.95% and 100%, respectively. It demonstrates that our method can effectively extract the span power lines from the segmentation results.

To further demonstrate the versatility of our search method across different types of pylons, we conduct experiments on four pylons with varying voltage classes and structures within the dataset. We select a segment that spans 6 m from the top to the bottom of the pylon to search for the axis of the symmetry equation. Fig. 11 illustrates the results of our search method and demonstrates that our search algorithms have achieved satisfactory results for all pylons.

### F. Separation of Individual Power Line Results

To evaluate the effectiveness of the separation module, we compare it with two methods. The first method is to manually separate a single power line from the span using the Cloud Compare software. The second method is to separate a single power line based on the DBSCAN method. Our separation module algorithm parameters are set to  $\{\text{res} = 1.0, \text{rate} = 0.6\}$  through the preliminary parameter experiment. In the evaluation

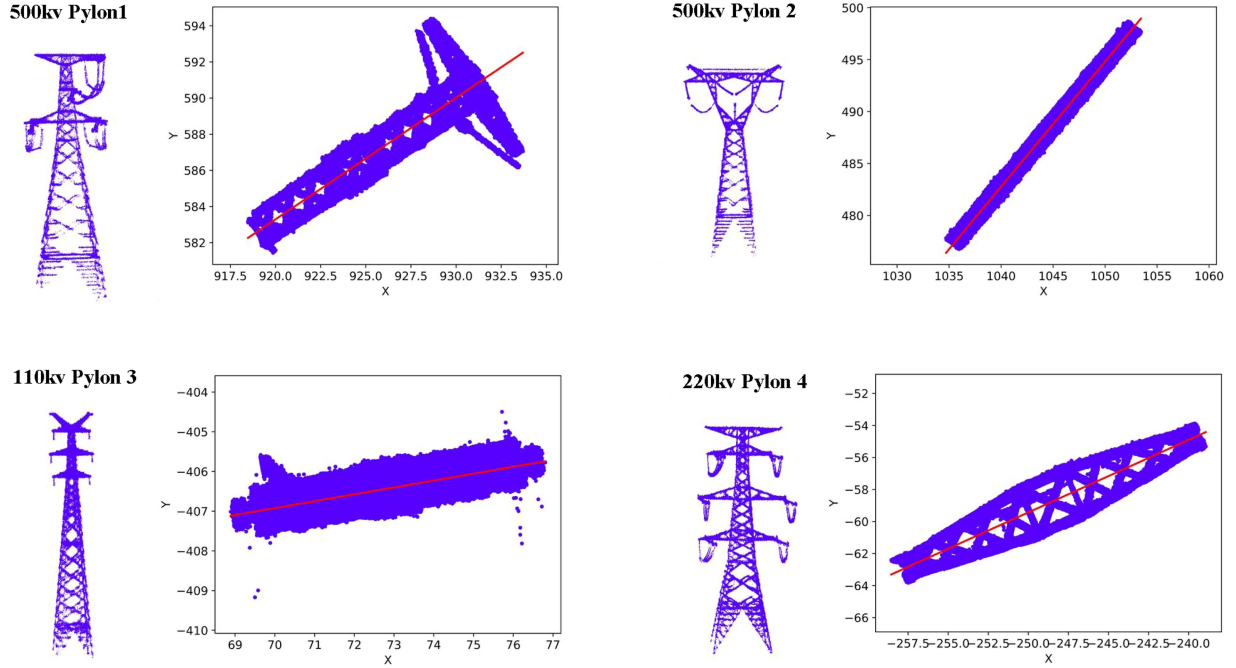


Fig. 11. Search results of the axis of symmetry equation in different pylons. Red lines are the equation found by our method in different types of pylons.

TABLE VI  
LPE (%) OF INDIVIDUAL POWER LINE EXTRACTION AND COMPUTATION TIME COMPARISONS IN SECOND (S)

Test Area	Number of Line	Points (mill.)	Cloud Compare		DBSCAN		Ours	
			LPE	LPE	Time	LPE	Time	
$S_0/T_0$	5	0.20	95.95	95.75	<b>40.6</b>	95.75	57.1	
$S_0/T_1$	5	0.10	96.52	96.32	<b>11.2</b>	96.32	25.3	
$S_1/T_0$	8	0.37	99.25	98.38	<b>137.8</b>	<b>99.25</b>	198.9	
$S_2/T_0$	9	0.85	95.00	83.37	804.3	<b>94.92</b>	<b>336.2</b>	
Average			96.68	93.46	/	96.56	/	

The best result are highlighted in bold.

criteria, the line point extraction rate (LPE) index is adopted to measure the separation effect of a single power line, and LPE is defined as follows:

$$\text{LPE} = \frac{1}{N} \sum_{i=1}^N \frac{\text{Num}_i}{\text{Num}_i^*} \quad (11)$$

where  $N$  denotes the number of individual power lines in a span area.  $\text{Num}_i^*$  represents the number of points on  $i$ th individual power line in the original scenario.  $\text{Num}_i$  represents the number of correctly extracted points on  $i$ th individual power line.

Table VI shows the comparison of the effects of each separation method. The power lines in  $S_0/T_0$  and  $S_0/T_1$  are relatively intact and connected. Therefore, the LPE of the three methods is close. However, in  $S_1/T_0$  and  $S_2/T_0$ , some individual power lines are broken to varying degrees, as shown in Fig. 12. LPE values of the DBSCAN method are reduced to 98.38% and 83.37%. Due to the constraint relation of the grid point stop condition, the LPE values of our method are 99.25% and 94.92%, almost identical to manual extraction.

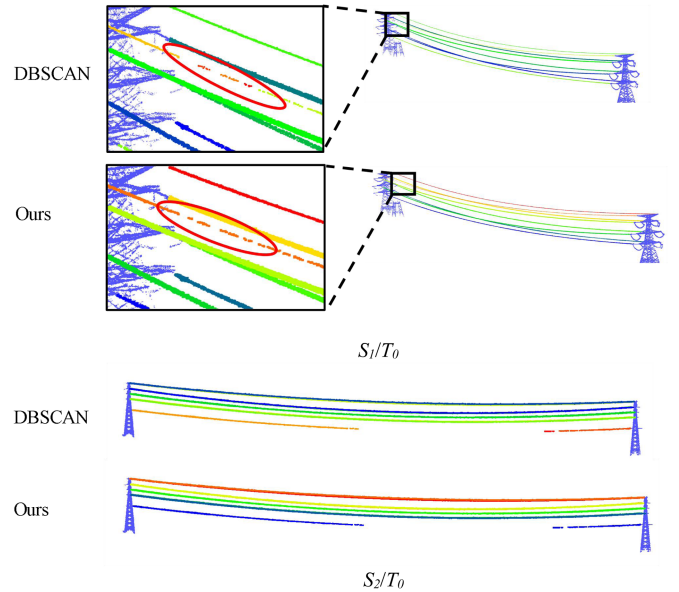


Fig. 12. Results of individual power line extraction.

In terms of efficiency, the time consumption of our algorithm is heavily influenced by the scale of power line points. For span power lines with a scale below 0.37 million, our algorithm does not exhibit a speed advantage. However, for span power lines with a scale of 0.85 million, our method exhibits a significant time consumption advantage. The primary reason is that the majority of computations in our method are concentrated on grid points instead of the vast number of power line points.



Fig. 13. Different disconnection states. (a) Disconnections in the middle. (b) Disconnections at the edge.

TABLE VII

LPE (%) VALUES FOR DIFFERENT DEGREES OF MISSING POWER LINE POINTS

	Case1		Case2	
	10%	15%	10%	15%
$S_1/T_0$	99.96%	99.92%	99.97%	99.96%

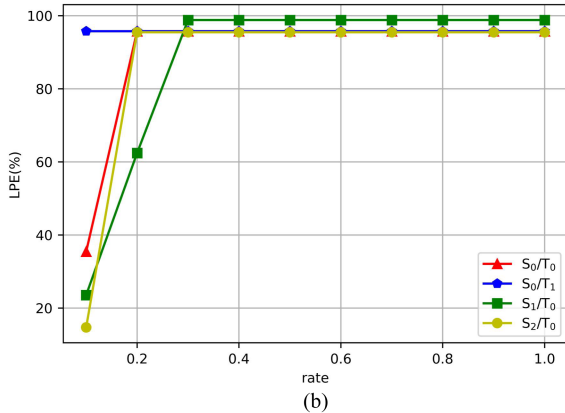
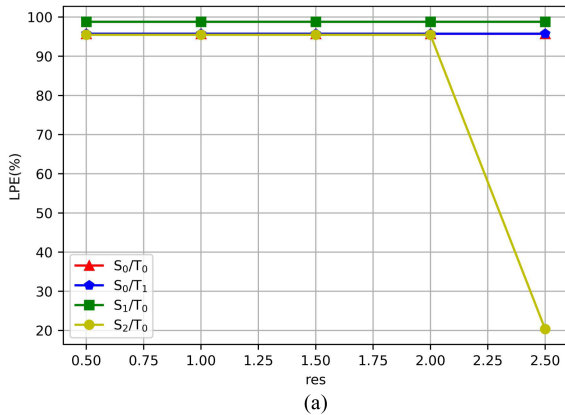


Fig. 14. Performance under different parameter settings. (a) *res*. (b) *rate*.

### G. Robustness Test

To verify the robustness of our individual power line separation algorithm under different missing power line point cases. We conduct experiments on  $S_1/T_0$ , which consists of different types of power lines, including both single conductors and bundled conductors. Two scenes are generated to simulate disconnections in the power lines: disconnections in the middle (Case1), and disconnections at the edge (Case2). In addition, scenes with disconnection rates ranging from 10% to 15% are created for both Case1 and Case2. The individual power lines in different colors shown in Fig. 13 are used as labels. Table VII shows the LPE values of different disconnection scenes. The

LPE values of all different scenes exceed 99%, indicating satisfactory results. These experiments demonstrate the robustness of our approach in different situations.

### H. Parameter Sensitivity Analysis on Individual Power Line Extraction

There are two essential parameters *res* and *rate* in individual power line extraction. In the experiment, one parameter is kept constant while the other varies within the optimization space to assess their sensitivity. After a number of test experiments, we preliminary found a favorable combination of parameters {*res* = 1.0, *rate* = 0.6}. The optimization space for *res* is set as {0.5, 1, 1.5, 2, 2.5}, and for *rate*, it is set as {0.1, 0.2, 0.3, 0.4, 0.5, 0.6, 0.7, 0.8, 0.9, 1.0}.

As shown in Fig. 14(a), while keeping *rate* = 0.6 and varying *res* within the range of [0.5, 2], LPE for power lines within four spans remains high. However, at *res* = 2.5, there is a significant drop in  $S_2/T_0$  performance, whereas the performance in other regions remains stable. Hence, lower values of *res* can provide greater robustness against the missing points problem. In terms of *rate*, when *res* is fixed at 1.0 and *rate* is less than 0.3, the performance across all regions is poor. When *rate* > 0.3, the performance remains stable, as shown in Fig. 14(b). Based on these results, the parameter combination can maintain the consistently high accuracy of LPE for power lines within four spans, while minimizing the negative impact of the missing point issue.

## IV. CONCLUSION

In this study, we have proposed an effective method for automatic semantic segmentation and individual power line extraction from electric power corridor point clouds for power line inspection. In the semantic segmentation stage, our method uses a specially designed LCM to improve the corridor semantic segmentation ability of SCF-NET. In the individual power line extraction stage, we use the symmetry axis equation of the pylon and the flexible grid to extract individual power lines. Our individual power line extraction method has shown a speed advantage when processing massive power line points. Experimental results show that the proposed methods achieve high accuracy in both stages. Specifically, the SCF-Net with LCM achieved a segmentation mIoU of 96.4%. In the extraction experiment, the LPE of all four spans is above 96.56%. The robustness test indicates the robustness of our method to missing power line point situation.

However, we acknowledge that some drawbacks still need to be addressed, such as the reliance on large datasets for training the segmentation model and the sensitivity of the flexible grid filter method to clutter points. Future work will focus on building a more generalized dataset and exploring instance-aware segmentation networks for end-to-end individual power line extraction.

## REFERENCES

- [1] L. Matikainen et al., "Remote sensing methods for power line corridor surveys," *ISPRS J. Photogrammetry Remote Sens.*, vol. 119, pp. 10–31, 2016.
- [2] X. Hui, B. Jiang, X. Zhao, and T. Min, "Vision-based autonomous navigation approach for unmanned aerial vehicle transmission-line inspection," *Int. J. Adv. Robot. Syst.*, vol. 15, no. 1, 2018, Art. no. 172988141775282.
- [3] T. He, Y. Zeng, and Z. Hu, "Research of multi-rotor UAV's detailed autonomous inspection technology of transmission lines based on route planning," *IEEE Access*, vol. 7, no. 99, pp. 114955–114965, Aug. 2019.
- [4] F. Azevedo et al., "LiDAR-based real-time detection and modeling of power lines for unmanned aerial vehicles," *Sensors*, vol. 19, 2019, Art. no. 1812.
- [5] W. Li, Z. Luo, Z. Xiao, Y. Chen, C. Wang, and J. Li, "A GCN-based method for extracting power lines and pylons from airborne LiDAR data," *IEEE Trans. Geosci. Remote Sens.*, vol. 60, 2022, Art. no. 5700614.
- [6] R. Zhang, B. Yang, W. Xiao, F. Liang, and Z. Wang, "Automatic extraction of high-voltage power transmission objects from UAV LiDAR point clouds," *Remote Sens.*, vol. 11, no. 22, 2019, Art. no. 2600.
- [7] J. Jung, E. Che, M. J. Olsen, and K. C. Shafer, "Automated and efficient powerline extraction from laser scanning data using a voxel-based subsampling with hierarchical approach," *ISPRS J. Photogrammetry Remote Sens.*, vol. 163, pp. 343–361, 2020.
- [8] W. Shi, "Fast and accurate power line corridor survey using spatial line clustering of point cloud," *Remote Sens.*, vol. 13, 2021, Art. no. 1571.
- [9] H. B. Kim and G. Sohn, "3D classification of power-line scene from airborne laser scanning data using random forests," *Int. Arch. Photogrammetry Remote Sens.*, vol. 38, pp. 126–132, 2010.
- [10] G. Bo, X. Huang, Z. Fan, and G. Sohn, "Classification of airborne laser scanning data using JointBoost," *ISPRS J. Photogrammetry Remote Sens.*, vol. 100, pp. 71–83, 2015.
- [11] Y. Liu, M. Aleksandrov, S. Zlatanova, J. Zhang, and X. Chen, "Classification of power facility point clouds from unmanned aerial vehicles based on Adaboost and topological constraints," *Sensors*, vol. 19, no. 21, 2019, Art. no. 4717.
- [12] Y. Wang, Q. Chen, L. Liu, D. Zheng, C. Li, and K. Li, "Supervised classification of power lines from airborne LiDAR data in urban areas," *Remote Sens.*, vol. 9, no. 8, 2017, Art. no. 771, doi: [10.3390/rs9080771](https://doi.org/10.3390/rs9080771).
- [13] A. Kamilaris and F. X. Prenafeta-Boldú, "Deep learning in agriculture: A survey," *Comput. Electron. Agriculture*, vol. 147, pp. 70–90, 2018.
- [14] X. Lu et al., "Multi-scale and multi-task deep learning framework for automatic road extraction," *IEEE Trans. Geosci. Remote Sens.*, vol. 57, no. 11, pp. 9362–9377, Nov. 2019.
- [15] R. Q. Charles, H. Su, M. Kaichun, and L. J. Guibas, "PointNet: Deep learning on point sets for 3D classification and segmentation," in *Proc. IEEE Conf. Comput. Vis. Pattern Recognit.*, 2017, pp. 77–85.
- [16] C. R. Qi, Y. Li, S. Hao, and L. J. Guibas, "PointNet++: Deep hierarchical feature learning on point sets in a metric space," in *Proc. 31st Int. Conf. Neural Inf. Process. Syst.*, 2017, pp. 5105–5114.
- [17] H. Zhao, L. Jiang, C. W. Fu, and J. Jia, "PointWeb: Enhancing local neighborhood features for point cloud processing," in *Proc. IEEE/CVF Conf. Comput. Vis. Pattern Recognit.*, 2019, pp. 5560–5568.
- [18] Q. Hu et al., "RandLA-Net: Efficient semantic segmentation of large-scale point clouds," in *Proc. IEEE/CVF Conf. Comput. Vis. Pattern Recognit.*, 2020, pp. 11105–11114.
- [19] S. Fan, Q. Dong, F. Zhu, Y. Lv, P. Ye, and F.-Y. Wang, "SCF-Net: Learning spatial contextual features for large-scale point cloud segmentation," in *Proc. IEEE/CVF Conf. Comput. Vis. Pattern Recognit.*, 2021, pp. 14499–14508, doi: [10.1109/CVPR46437.2021.01427](https://doi.org/10.1109/CVPR46437.2021.01427).
- [20] F. Shuang, P. Li, Y. Li, Z. Zhang, and X. Li, "MSIDA-net: Point cloud semantic segmentation via multi-spatial information and dual adaptive blocks," *Remote Sens.*, vol. 14, no. 9, 2022, Art. no. 2187, doi: [10.3390/rs14092187](https://doi.org/10.3390/rs14092187).
- [21] B. Hga et al., "UAV-LiDAR aids automatic intelligent powerline inspection," *Int. J. Elect. Power Energy Syst.*, vol. 130, 2021, Art. no. 106987.
- [22] C. Silva, A. Pacheco, S. Valente, and J. Centeno, "Automatic extraction of power transmission lines using laser scanner data," *J. Remote Sens. Technol.*, vol. 3, pp. 46–54, Nov. 2015, doi: [10.18005/JRST0304001](https://doi.org/10.18005/JRST0304001).
- [23] H. Guan, J. Li, Y. Zhou, Y. Yu, C. Wang, and C. Wen, "Automatic extraction of power lines from mobile laser scanning data," in *Proc. IEEE Geosci. Remote Sens. Symp.*, 2014, pp. 918–921, doi: [10.1109/IGARSS.2014.6946575](https://doi.org/10.1109/IGARSS.2014.6946575).
- [24] M. Lehtomaki, A. Kukko, L. Matikainen, J. Hyyppa, H. Kaartinen, and A. Jaakkola, "Power line mapping technique using all-terrain mobile laser scanning," *Automat. Construction*, vol. 105, 2019, Art. no. 102802.
- [25] C. Peng, L. Yang, S. Shi, W. Zhang, and H. Du, "Research on power line segmentation and tree barrier analysis," in *Proc. 3rd Int. Conf. Electron. Inf. Technol. Comput. Eng.*, 2019, pp. 1395–1399, doi: [10.1109/EITCE47263.2019.9094966](https://doi.org/10.1109/EITCE47263.2019.9094966).
- [26] W. Mao, C. Wang, J. Wang, J. Zhou, and Y. Mai, "Extraction of power lines from laser point cloud based on residual clustering method," *Acta Geodaetica et Cartographica Sin.*, vol. 49, pp. 883–892, 2020.
- [27] C. Chen, B. Yang, S. Song, X. peng, and R. Huang, "Automatic clearance anomaly detection for transmission line corridors utilizing UAV-borne LiDAR data," *Remote Sens.*, vol. 10, no. 4, 2018, Art. no. 613.
- [28] S. Shi, L. Yang, K. Chen, F. Chen, S. Lei, and L. Liu, "A method of power line hanging point location based on LiDAR data," in *Proc. IEEE 3rd Adv. Inf. Manage., Communicates, Electron. Automat. Control Conf.*, 2019, pp. 1900–1905, doi: [10.1109/IMCEC46724.2019.8984162](https://doi.org/10.1109/IMCEC46724.2019.8984162).
- [29] C. L. Perrin, "Numerical Recipes in Fortran 90: The Art of Scientific Computing, second edition, volume 2 (3 CD-ROMs and manual) by William H. Press, Saul A. Teukolsky, William T. Vetterling, and Brian P. Flannery. Cambridge University Press: New York, 1996," *J. Amer. Chem. Soc.*, vol. 119, no. 37, pp. 8748–8748, 1997.
- [30] Q. Shi, S. Anwar, and N. Barnes, "Semantic segmentation for real point cloud scenes via bilateral augmentation and adaptive fusion," in *Proc. IEEE/CVF Conf. Comput. Vis. Pattern Recognit.*, 2021, pp. 1757–1767.



**Xiuning Liu** received the B.S. degree in mechanical engineering from Ningbo University, Ningbo, China, in 2018. He is currently working toward the M.Sc. degree in pattern recognition and deep learning, at the Intelligent Robot Research Center, School of Electrical Engineering, Guangxi University, Guangxi, China.

His research interests include electric power corridor point cloud processing and intelligent processing of point clouds.



**Feng Shuang** received the bachelor's degree in mathematics and physics from the Special Class of Gifted Young, University of Science and Technology of China (USTC), Hefei, China, in 1995, and the Ph.D. degree in chemical physics from the Department of Chemical Physics, USTC, in 2000.

He once worked with the Institute of Intelligent Machines (IIM) and the University of Science and Technology of China (USTC) as the Director of the Robot Sensor Laboratory. From 2001 to 2003, he was a Research Associate with Princeton University, where he was also a research staff member from 2004 to 2009. In 2009, he joined IIM as a Full Professor. Since 2018, he has been the Dean of the School of Electrical Engineering, Guangxi University, Nanning, China, where he is also a Professor. He has authored/coauthored more than 60 papers and applied for more than 10 national invention patents. His research interests include intelligent mobile robots, multidimensional force sensors, quantum system control, etc.

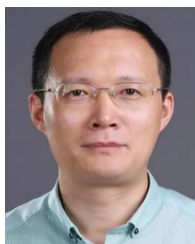
Prof. Shuang was selected as a Member of the "One Hundred Talented People of Chinese Academy of Sciences."



**Yong Li** received the Ph.D. degree in pattern recognition and intelligent systems from Northeastern University, Shenyang, China, in 2020.

He is currently an Assistant Professor with the School of Electrical Engineering, Guangxi University, Nanning, China. His research interests include intelligent robots, point cloud processing, computer vision, and pattern recognition.





**Liqiang Zhang** received the Ph.D. degree in geoinformatics from the Institute of Remote Sensing Applications, Chinese Academy of Sciences, Beijing, China, in 2004.

He is currently a Professor with the Faculty of Geographical Science, Beijing Normal University, Beijing, China. His research interests include remote sensing image processing, three-dimensional urban reconstruction, and spatial object recognition.



**Jianchuang Qin** received the bachelor's degree in automation from the Wuhan University of Technology, Wuhan, China, in 2021. He is currently working toward the M.Sc. degree in artificial intelligence at the Intelligent Robot Research Center, School of Electrical Engineering, Guangxi University, Guangxi, China.

His research interests include mobile laser scanning and point cloud instance segmentation.



**Xingwen Huang** received the B.S. degree in electrical engineering from the Hefei University of Technology, Hefei, China, in 2019. He is currently working toward the postgraduate degree in pattern recognition and deep learning at the Department of Electrical Engineering, University of Guangxi, Nanning, China.

His research interests include intelligent electric power inspection and point cloud semantic segmentation.